Comparison of Three Strategies for Buzz-saw Noise Propagation in an Aeroengine Intake with Flow Distortion using CFD

Joseph S. P. Binns*, Long Wu[†] and Alexander G. Wilson[‡] *Institute of Sound and Vibration Research, University of Southampton, Highfield, Southampton, UK SO17 1BJ*

The expense of computational methods that can accurately predict the tonal acoustic field in an aeroengine intake is a current limitation for understanding current and future challenges in aeroengine noise, such as the impact of increased flow distortion with UHBR (Ultra-High Bypass Ratio) turbofan designs. In this study, the intake propagation of shock-associated fan tone noise through a distorted inflow is considered. Three numerical methodologies are applied to explore novel methods for reducing the computational demand of representative and accurate calculations. The datum case considers the full intake domain with a fully structured computational mesh. A part-span approximation neglects low-span regions of the duct according to the observation that most of the interested acoustic content has energy focused towards the outer walls of the duct. Finally, a hybrid technique combines the earlier approaches by filling the previously neglected space with unstructured mesh. Both the part-span and hybrid methodologies unlock considerable computational savings. Both cases could sufficiently resolve the distorted flow field. The acoustic field at the first two Blade Passing Frequencies (BPFs) was considered for all cases. At the first BPF, both methodologies successfully represent the highest amplitude components. At the second BPF, more deviations were observed for the case that applied the part-span approximation, while the hybrid case results matched well with the datum case.

I. Nomenclature

BPF = Blade Passing Frequency

BPR = Bypass Ratio

CAA = Computational AeroAcoustics CFD = Computational Fluid Dynamics

EO = Engine Order

ESS = Engine Stator Section

FFT = Fast Fourier Transform

FPR = Fan Pressure Ratio

LBM = Lattice Boltzmann Method

MPT = Multiple Pure Tones

OGV = Outlet Guide Vane

(U)RANS = (Unsteady) Reynolds Averaged Navier-Stokes

UHBR=Ultra-High Bypass RatioB=Number of bladesV=Number of stator vanes Ω =Angular frequencyM=Mach Number

L/D = Intake length-to-diameter ratio

r = Radial position θ = Azimuthal position z = Axial position

^{*}PhD Candidate, J.Binns@soton.ac.uk.

[†]Research Fellow.

[‡]Professor of Computational Aeroacoustics.

m = Azimuthal mode index n = Radial mode index c_0 = Speed of sound v = Hub-tip ratio

II. Introduction

Atto grow and environmental regulations become ever-stricter [1, 2]. A complex noise profile varying under different operating conditions further complicates this challenge and continues to warrant research and developments by industry and academia. For large passenger and cargo aircraft, high-bypass-ratio turbofan engines are the current propulsion system of choice due to their efficiency and relatively low noise profile. Nevertheless, tonal noise contributions from the fan system are generally dominant in the forward arc during take-off, the initial climb and cutback conditions. At the approach condition, Rotor-Stator Interaction (RSI) tones are usually smaller than broadband components but can still be significant.

The further requirement for increased sustainability and fuel efficiency has promoted higher bypass ratios and lower fan pressure ratios in future designs, leading to Ultra-High ByPass Ratio (UHBR) designs [3, 4]. To maintain reasonable weight and drag characteristics, these engine designs are more compact, resulting in intake regions that are shorter relative to the fan diameter. Hence, it is anticipated that the amount of inflow non-uniformity in the intake duct and observed by the fan will increase, which has the potential to impact fan performance [5] and has been shown to impact tone noise source and propagation mechanisms [6–16]. This study focuses on the latter point, particularly addressing the high computational demand of accurate numerical predictions for the propagation of tone noise in the intake.

Shock-associated fan tone noise is a dominant noise source at high-power operating points and arises when shock waves form near the leading edge of each blade as a result of supersonic tip speeds. This induces a high-amplitude cut-on pressure field that propagates non-linearly upstream through the intake. The shocks rotate with the fan (rotor-locked) and, according to weak shock theory, propagate at the undisturbed speed of sound relative to the oncoming flow [17] for a uniform inflow condition. Identical blades produce the same pressure oscillation at each blade passage, leading to tonal noise at the Blade Passing Frequency (BPF) and its harmonics only. In practice, there are small blade-to-blade variations due to manufacturing tolerances and wear. Particularly significant for shock generation is the variation in stagger angle that changes the flow capacity and the shock-detachment distance for each blade passage, affecting both the shock strength and propagation angle [18]. The consequent pressure field varies between each blade passage and repeats every full rotation of the fan, resulting in tonal components at every multiple of the fan rotation speed, or Engine Order (EO). This form of fan tone noise is often termed Multiple Pure Tones (MPT) or, as in this study, buzz-saw noise.

Computational approaches that can accurately resolve buzz-saw noise source generation and propagation are currently too expensive to be applied iteratively during the design process. Other more affordable approaches are available (as discussed in the following section), but often make significant assumptions such as linearity and/or geometric simplifications, making them insufficient for complex cases, such as those where buzz-saw noise propagation through distorted flow is concerned.

We previously introduced a part-span approximation [19, 20] for linear and non-linear propagation of tone noise in aeroengine intakes. The approximation utilises the observation that for the tone noise present in an aeroengine intake, much of the acoustic energy flux is concentrated towards the outer wall of the duct. Hence, the part-span approximation allows for a reduction in the size of the computational domain by neglecting the low-span regions of the intake duct. This work highlighted the potential computational savings and predicted the acoustic pressure field with reasonable accuracy. However, the analysis was limited and the present study aims to address this, as is explained in more detail in the scope of the study section.

A. Prediction methods

Non-linear three-dimensional Computational Fluid Dynamics (CFD) calculations represent the most comprehensive computational method for predicting acoustic source and propagation mechanisms in aeroengines. Unsteady Reynolds-Averaged Navier-Stokes (URANS) simulations can account for non-uniform flow, realistic geometries, and installation effects but demand high computational resources. RANS methods decompose the flow field into averaged and fluctuating components, replacing the turbulent stress term in the Navier-Stokes equations with a turbulence-model-dependent term. The inclusion of an unsteady term in the momentum equation enables URANS computations. Doherty and Namgoong

[9] validated URANS for noise predictions in installed turbofan intakes with 3D inflow effects, while Daroukh et al. [14] extended this to include upstream and downstream flow non-uniformities, resolving tonal noise up to the second blade passing frequency (BPF) at a cost exceeding 1 million CPU hours. Wu and Wilson [16] applied URANS to study shock-associated noise propagation through steady distorted flow, resolving up to the third BPF using a 200-million-cell mesh, and requiring significant computational resource.

The Lattice Boltzmann Method (LBM) offers an alternative approach, modeling flow via microdynamics rather than continuum assumptions [21]. Gonzalez-Martino and Casalino [22] demonstrated LBM's capability for transonic turbofan noise prediction, with applications achieving reasonable broadband and tonal accuracy [22, 23], albeit with substantial computational costs. Demonstrations have achieved reasonable predictions of broadband spectra at subsonic conditions and tonal components at transonic regimes. The full Euler formulation has been demonstrated for the prediction of aeroengine noise, also accounting for non-linear propagation effects close to the fan [24].

Linear computational approaches are often applied for predicting aeroengine tone noise propagation according, and are reviewed in detail by Astley et al. [8]. The frequency-domain Finite Element/Infinite Element (FE/IE) method, based on the convected Helmholtz equation, is commonly used [10, 25]. It is effective for intake propagation and radiation predictions at frequencies of interest in large acoustic domains but is based on an acoustic velocity potential and is difficult to implement for rotational flow. The computational expense of FE/IE methods, which is memory limited, rapidly increases with problem size making large three-dimensional cases expensive [26]. Time-domain approaches include high-order finite difference [27], compact Dispersion Relation Preserving (DRP) schemes [28], and the Discontinuous Galerkin Method (DGM) for Linearized Euler Equations (LEE) on unstructured grids [29]. While DGM's flexibility suits complex geometries, its linear assumptions are inadequate for high-amplitude non-linear propagation in intakes. The non-linear region is generally limited to a portion of the intake but is significant for shock noise propagation. Adjustments to linear Computational Aeroacoustics (CAA) approaches can be made to partially account for non-linearity, such as those based on the analytical model introduced by Morfey and Fisher [30] and extended by Fisher et al. [31] and then in a series of studies from McAlpine and Fisher [17, 32–35].

Eigen analysis methods have long been used to understand duct acoustic propagation. Tyler and Sofrin's [36] work on aeroengine tone noise is based on eigen analysis of uniform annular cylindrical ducts with uniform axial mean flow. Their work is still widely used to attain general estimates but has limitations making it insufficient in many cases. In realistic situations, aeroengine intake ducts are not uniform, flow is generally non-uniform radially (and in many cases azimuthally), and significant non-linear effects can often not be ignored. Rienstra [37] combined the eigenvalue approach with a multiple-scales methodology to accommodate annular cylindrical ducts of slowly-varying radius. The Eigen Analysis in General Curvilinear Coordinates (EAGCC) method, introduced by Wilson [38], is an eigen analysis method for the propagation and modal decomposition of linear acoustic flow disturbances that can account for variations in mean flow as well as non-uniform, yet smoothly varying ducts and has been demonstrated for understanding the acoustic field in an aeroengine intake [39]. Eigen analysis methods are computationally faster than more conventional methods, such as a RANS CFD calculation, though are still generally limited by linear approximations. Wilson [40] successfully extended his EAGCC model for two-dimensional non-linear propagation but highlighted the increased complexity of such predictions, indicating that further extension to three-dimensional flow/geometry would be significantly more laborious.

Far-field radiation is not considered in the present study.

B. Impact of Steady Flow Distortion

Future Ultra High Bypass Ratio (UHBR) designs [3, 4] feature shorter intakes to reduce weight and drag, limiting the effectiveness of acoustic liners in the intake and potentially increasing the amount of flow distortion through the intake and at the fan. Early studies of fan tonal noise focused on noise source and propagation mechanisms with undisturbed/uniform flow [8, 17, 18, 30, 32–35, 41–43]. The presence of flow distortion has been increasingly included in more recent studies.

Experimentally, challenges arise in generating realistic distortion profiles. Schwaller et al. [6, 7] is an example of experimental work who considered steady inflow distortion introduced by intake geometry with an in-situ model. A modal scattering effect was observed for the drooped intake case during propagation. Inflow distortion, typically described by low-order azimuthal modes k [12, 44], interacts with rotor-locked pressure fields to produce scattered modes $m = nB \pm k$, resulting in a pressure field consisting many azimuthal modes, each with variations in amplitude and phase [45]. This effect was identified in Schwaller er al.'s [6, 7] by a microphone array at a single position upstream in the intake, and hence the physical understanding was limited.

Computational studies provide a more complete representation of flow and acoustic fields compared to experimental approaches, employing various numerical methods including non-linear CFD [9, 13, 14, 44], linear Computational Aeroacoustics (CAA) [10], and hybrid coupling techniques [12, 46–48]. Some studies decouple source and propagation effects for tractability but as a result can neglect important coupling effects, while coupled simulations face challenges in isolating the mechanisms and many employ simplifications that neglect critical physical mechanisms.

Doherty and Namgoong's [9] URANS study of a drooped intake with sliding-mesh fan coupling revealed significant circumferential flow variations under distortion. The non-uniform relative Mach number and inlet angle for each blade led to shock-strength variations, producing axially and circumferentially varying Fourier amplitudes at the first BPF. Rotor-locked modes scattered into neighbouring modes both at source and during propagation through the distorted field. A substantial portion of the work was validating the method with experimental data from a model fan rig where good agreement was observed. This simulation was considered 'state-of-the-art' and was designed for noise predictions up to the third BPF, though only validation at the first BPF was presented.

Daroukh et al. [11, 14] demonstrated a fully installed numerical solution for turbofan tonal noise through studies incorporating both drooped intakes and heterogeneous OGV rows with struts and pylons. At subsonic regimes [11], their Rotor-Stator Interaction (RSI) analysis demonstrated 3 dB noise increases due to distortion. For transonic operating points [14], they identified the inadequacy of Tyler-Sofrin (TS) modes [36] to fully describe the tonal acoustic field when distorted flows are present. The research identified shock position variability along blade chords and unsteady loading variations across blades. Another study by Daroukh et al. [15] considered a uniformly staggered fan, meaning the shock pattern was uniform across the blade row for the undistorted case, inducing the rotor-locked m = nB modes only. For the distorted case, the azimuthal mode distribution at the BPF was shown to vary considerably. Close to the fan, the rotor-locked mode was scattered into nearby neighbouring modes and had significant amplitude. After propagating through the distorted intake flow field, modal scattering into more distant azimuthal components was observed.

Winkler et al. [12] employed a hybrid CFD/CAA approach introduced by Winkler et al. [48], to predict the impact of a 3D drooped nacelle geometry on inlet and aft noise. The static test bed conditions meant flow distortion was introduced by inlet asymmetry and a heterogenous OGV row with bifurcations. The intake distortion could be well characterised by low-order azimuthal modes, while the downstream distortion had more complex modal contributions, albeit at a relatively lower amplitude. Their analysis tracked the evolution of different modal components at the first BPF both upstream and downstream. TS modes were dominant downstream but decayed quickly upstream of the fan. In the intake, the distortion interaction modes contributed significantly to the pressure field. This study highlighted the requirement for coupled and installed aeroengine noise simulations to accurately represent the acoustic field, but test conditions meant it was not representative of an in-flight case.

Wu and Wilson [16] completed a numerical study considering fan buzz-saw noise with intake flow distortion. An axisymmetric and drooped intake were considered with a shallow in-flight angle of attack and a non-uniformly staggered blade row. A Fourier-Bessel wavesplitting method, introduced by Wilson [49], was used to analyse the acoustic field. The shallow angle of attack, in conjunction with a more conventional intake geometry and a relatively large length-to-diameter ratio meant that close to the fan, the observed impact of distortion was low. More significant was the impact of circumferentially inhomogeneous flow in the intake during upstream propagation of the noise. A circumferential mode scattering effect was highlighted in the distorted cases, most significantly in the drooped intake case, where a higher level of distortion was observed.

Prinn et al.'s [10] linear CAA study demonstrated that even low-level distortion significantly scatters BPF tones into adjacent circumferential modes by the intake throat. The far-field propagation study found that the distortion had a significant effect on the directivity of propagated noise. For the drooped intake, the noise was directed more skywards and to the sides. These findings aligned with Astley et al.'s [50] semi-analytical work which also considered the effect in acoustically lined ducts.

C. Previous work

To address the high computational demand of CFD simulations that can resolve high-amplitude shock-associated tonal noise propagation in an aeroengine, our recent work [19, 20] introduced a 'part-span approximation'.

The part-span approximation exploits the observation that, at high-power operating conditions, much of the acoustic energy flux in the intake is concentrated near the duct outer walls. By neglecting low-span regions and resolving only the flow from an artificial hub wall to the outer duct wall, this approach offers significant computational savings. Our previous studies have both demonstrated its potential and characterised its limitations for both linear and non-linear propagation.

Application of the part-span approximation for linear propagation highlighted that for most applied cases (such as for BPF acoustic modes), minimal error is introduced. However, in some specific cases, the error introduced could be significant and was categorised into:

- Source truncation errors relating to the amount of acoustic energy truncated by the part-span approximation,
- In-duct propagation errors relating to differences in axial wavenumber introduced by the part-span artificial inner wall, and
- Far-field radiation errors relating to differences observed in the far field.

Source truncation errors were most significant for low-order azimuthal modes where the distribution of acoustic energy is spread across a larger span of the duct. In-duct propagation errors were most significant for modes close to the cut-off/cut-on ratio, where the presence of a part-span approximation could change the state of the mode. As a result, the linear analysis highlighted that most care should be taken when the acoustic content of interest satisfies one, or both, of these conditions. Much of the analysis in this study included significant approximations regarding intake duct geometry and mean flow conditions, as well as being limited to linear propagation. It was anticipated that the error introduced hence becomes even more complex when more realistic cases are considered.

This was briefly supported by the application of the part-span approximation for non-linear propagation of buzz-saw noise through an axisymmetric, but otherwise realistic, intake with non-zero angle of attack inflow conditions [20]. The analysis in this study was limited to modal descriptions of the acoustic field at two discrete axial positions in the intake. While brief, this analysis indicated that the impact of distortion on the acoustic field could be resolved at the first BPF, where a mode scattering effect was observed. However, some significant deviations were observed, particularly at low engine order (EO) frequencies, as was anticipated by the prior linear analysis. Furthermore, radial mode interference was observed through the duct in the datum case, which could not be accurately resolved by the part-span approximation due to the change in geometry. The significance of this would be case dependent but, nevertheless, this effect was highlighted as a potential limitation.

The non-linear study was useful to demonstrate the application of the part-span approximation, but the study itself had several limitations that flawed the comparison:

- Comparative cases used different numerical solvers, meaning that highlighting error between the cases was not
 conclusive, particularly due to the presence of shockwaves which can be very sensitive to solver-specific shock
 dissipation schemes.
- The reference full-span case employed a coupled fan-intake domain, meaning that some source effects may have been omitted by the part-span case.
- Analysis was restricted to azimuthal mode distributions at limited axial stations, as discussed.

These limitations are addressed in the present study to better evaluate the part-span approximation and another meshing methodology, as explained in the following section.

D. Scope of the paper

The primary barrier to understanding aeroengine shock-associated tonal noise in the intake is the high computational cost of aeroacoustic simulations capable of resolving the acoustic field with sufficient accuracy. While conventional approaches using high-quality, fully structured meshes have been validated, they demand prohibitive computational resources for the preliminary design process.

This study evaluates three meshing methodologies for URANS-based CFD simulations to improve computational efficiency while maintaining accuracy:

- Conventional fully structured mesh: Serves as the baseline validated approach, providing a reference solution.
- **Part-span approximation**: As described in the previous section, this approach uses a fully structured mesh in the part-span domain and neglects low span regions in the duct to reduce computational expense.
- **Hybrid structured-unstructured mesh**: An approach that bridges the gap between a conventional and part-span methodology by:
 - Maintaining high-quality structured mesh towards the outer wall of the intake duct.
 - Implementing an unstructured mesh zone in low-span duct regions
 - Extending unstructured mesh to the far-field boundaries for additional computational savings

The current work focuses specifically on tonal noise propagation, considering an undistorted acoustic source propagating through a steady distorted mean flow. Following validation against the conventional approach, a two-part *source-propagation* methodology is proposed in later sections, allowing for the impact of distortion on the source to be included.

This paper will also begin to understand the evolution of the acoustic field through the intake, considering the impact of steady flow distortion on high-amplitude tonal noise propagation.

III. Turbofan Geometry and Operating Conditions

In this study, a full-scale, axisymmetric yet otherwise realistic intake geometry with a ratio of intake length to duct diameter (L/D) of around 0.53 is used. The source calculation is not presented in this study but used a fan stage with B=22 fan blades. To mimic the blade-to-blade manufacturing deviation, typical individual stagger angle variations are imposed at the tip of each rotor blade and then linearly vanish to zeros at the blade hub. Only homogeneous Outlet Guide Vanes (OGVs) and Engine Stator Sections (ESSs) are considered, since shock-associated tone noise is the focus of the current study.

For the source simulation, the fan was operating in the transonic region and the rotation speed was set to 89% of the nominal value. A flight Mach number of $M_{\infty} = 0.4177$ was used and the static pressure and temperature were determined by isentropic flow relations based on the ambient atmospheric conditions at a given flight altitude. For the source calculations, the flight angle of attack was set to AoA = 0 degrees. For the calculations presented in this study, the flight conditions were the same, other than a non-zero flight angle of attack of AoA = 3.57 degrees. Consequently, the source and propagation are decoupled and only the distortion-propagation effect is understood in this study. For the present geometry and operating conditions, Wu and Wilson [16] observed that the impact of distortion at the source was almost negligible, meaning the use of an undistorted source is reasonable in this case. This also highlights that any known source can be implemented in the present methodologies, which may be a benefit for parametric-based studies, such as the investigation of different acoustic liner configurations.

IV. CFD Method

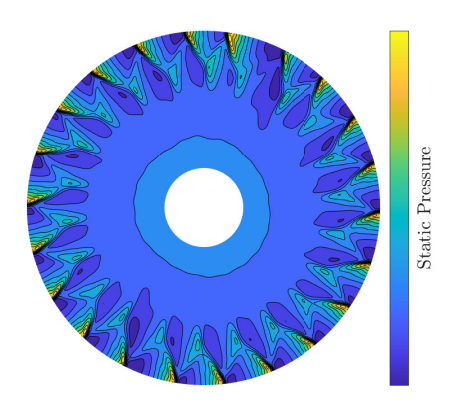
Three-dimensional unsteady RANS (Reynolds-Averaged Navier-Stokes) equations were solved using the commercial software Ansys Fluent. Second-order upwind spatial and second-order implicit temporal discretisation schemes were applied. The Spalart-Allmaras turbulence model was used in accordance with other similar turbomachinery applications [9, 51, 52].

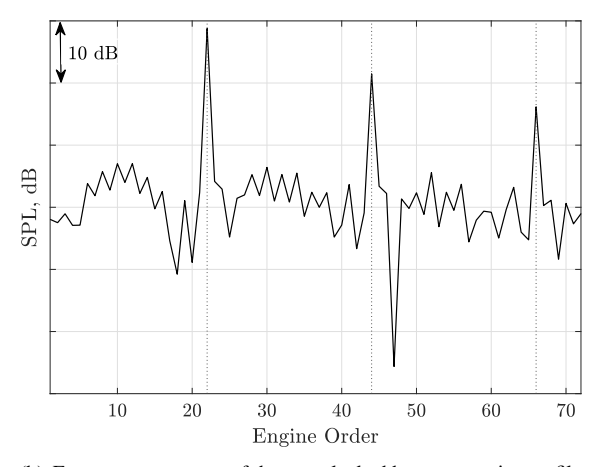
The source calculation is not presented in this paper but has been introduced in the previous sections and is fully described by Wu and Wilson [16].

The method for the propagation calculations implements an unsteady static pressure boundary condition at the source plane, which is just upstream of the fan leading edge. A full source rotation is resolved by 1600 outer time steps with 10 inner iterations for each time step. Viscous boundary conditions are used for the intake wall and spinner. For the part-span domain, an inviscid boundary condition is used for the domain wall, which is further explained in the following section. The flow conditions were specified at the upstream and adjacent external boundaries using free-stream characteristic boundary conditions, specifying the static pressure, Mach number, flow direction and total temperature. An unsteady boundary condition was implemented at the downstream source boundary (fan-face). After each time step, the boundary was updated with a static pressure profile. The source data was acquired in the study of Wu and Wilson [16] and was resolved in a URANS simulation with the same intake geometry as that in the present study. The source was resolved for an undistorted case, that is with an axisymmetric intake geometry and a zero-degree inflow angle. Consequently, any impact of distortion observed in the later results section is wholly due to propagation effects.

Figure 1(a) shows a static pressure contour plot of the source used for the simulations in this study, obtained by Wu and Wilson [16]. The full-span profile is shown, and the same profile is used for each methodology. Figure 1(b) presents the Engine Order (EO) spectrum of the source, computed at 99% span. Given the source has no impact of distortion included, the spatial and temporal (over a full revolution) Fourier spectra (at the same radial positions) are identical. Distinct peaks at each BPF (a dotted line highlights the first three) can be observed, as well as varying amplitudes at different EO's due to the non-uniform stagger variation of the fan present in the source simulation.

The unsteady pressure field was monitored at different positions in the intake to determine the unsteady convergence of the present simulations. After 10 full source revolutions, unsteady convergence was observed in all cases. The unsteady solutions were then transformed into the frequency domain at discrete frequencies for subsequent revolutions according to a Fast Fourier Transform (FFT). The first two Blade Passing Frequencies (BPFs) are considered in the present study. Solutions from each case are interpolated onto regular grids for analysis purposes. A Fourier-Bessel mode decomposition was completed on the acoustic field as an analysis tool. The acoustic modes obtained by this method assume a uniform axial flow. As a result, they do not directly relate to the actual acoustic modes present in a





- (a) Static pressure contour plot at the source plane in the duct.
- (b) Frequency spectrum of the rotor-locked buzz-saw noise profile used as the source of the present calculations. The spectrum was completed at 99% span and is presented in terms of Engine Order (EO).

Fig. 1 A contour and frequency spectrum of the source pressure field used for the present calculations. The source is known and was obtained during a series of URANS simulations, as presented by Wu and Wilson [16].

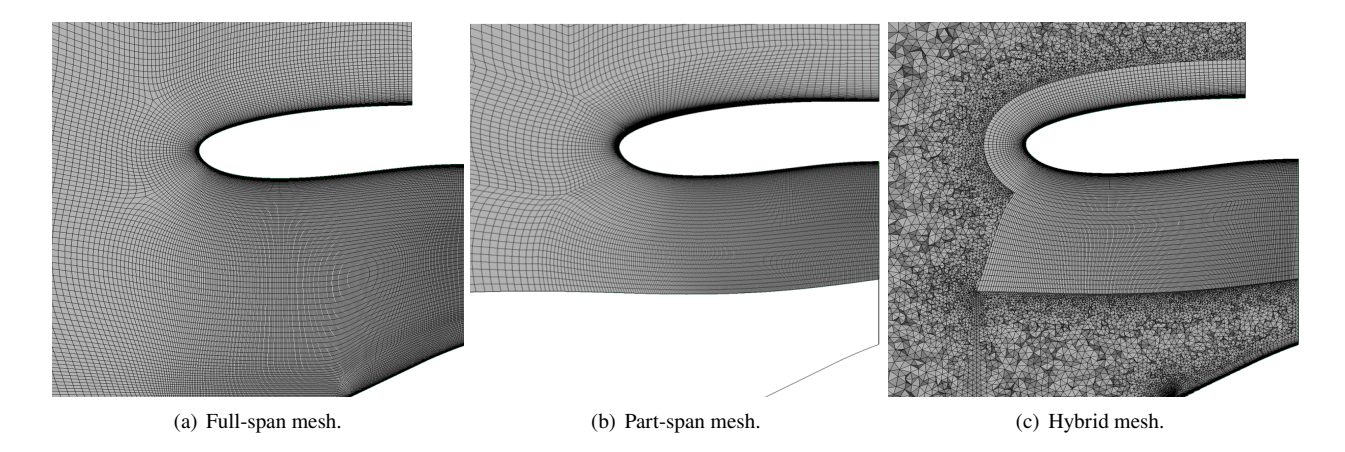


Fig. 2 A cross-section view of each meshing approach used throughout the study.

distorted flow case. Nevertheless, they are used to develop an understanding of the acoustic field and are commonly used for coupling with CAA methods and acoustic liner design. A full 3D modal decomposition will be completed in a later study.

V. Computational Methodologies

As mentioned, three methodologies are presented in this study:

- A Conventional 'full-span' (datum case)
- B 'Part-span'
- C Hybrid meshing

Figure 2 shows an azimuthal plane of the computational mesh in the intake duct used for each methodology,

A. Conventional 'full-span' methodology

The conventional 'full-span' methodology considers the intake region as a single domain, capturing the whole flow field in a stationary reference frame. The downstream extremity is the source position and is geometrically around 0.04

fan diameters upstream of the fan leading edge. Viscous wall boundary conditions were used for the nacelle and spinner, where the spinner was rotating at a speed according to the rotational frequency of the fan.

The computational mesh is fully structured and has a near wall Y+ of order one. The intake mesh has the same topology as the intake domain mesh presented by Wu and Wilson [16]. It has around 110 million cells and is the largest mesh considered in this study. Hence, it is computationally most expensive and is the datum case. In practice, a full-span approach is widely used and has demonstrated reasonable predictions for tonal fan noise with flow distortion.

B. 'Part-span' methodology

First introduced by Binns et al. [19, 20], the 'part-span' approximation utilises the observation that most of the interested acoustic content in an intake duct has acoustic energy focused towards its outer walls. As a result, the approximation neglects low-span regions in the duct. Geometrically throughout the duct, a streamtube according to the intake mean flow is generated with a given hub-tip ratio ν at the source plane. In this case, the hub-tip ratio applied is $\nu = 0.5$, where streamtube seeds are placed and propagated upstream. Numerically, this boundary is treated as an inviscid slip wall and hence has no impact on the flow.

The approximation allows for a considerable reduction in the computational mesh size, with around 78 million cells. This computational mesh is also fully structured, follows the same blocking topology as in the full-span case, and has a near wall *Y*+ of order one.

This approximation has been previously considered for the same operating conditions as in this paper [20], though post-processing of the data was limited to instantaneous snapshots and a limited amount of probe data in the domain. Furthermore, in our previous study, the part-span approximation was compared with data which was resolved in a different numerical CFD solver and also implemented a coupled fan-intake domain. The present study offers a more representative comparison and evaluation of the part-span approximation.

C. Hybrid meshing methodology

The hybrid meshing methodology aims to bridge the gap between the previous two methodologies. The philosophy is to maintain a regular, high-quality structured mesh in the high-span regions of the duct where the acoustic content is of most interest while using unstructured cells in the rest of the domain to reduce the overall cell count and maintain a numerical solution of the entire domain.

In the duct, a streamtube defines the interface between fully unstructured cells and the h-block. Upstream of the intake highlight, the domain is discretised in a fully unstructured way. The c-block around the nacelle wall has the exact resolution as in the other approaches with a near-wall Y+ of order one. In the h-block, a semi-structured topology is employed where, in the azimuthal direction, the resolution is reduced by a factor of three before reaching the streamtube interior boundary. This maintains a suitable resolution for the acoustic content as the geometric spacing between cells in this direction decreases as the radius reduces. This also allows an orthogonal interface mesh between the h-block and unstructured region to be achieved, allowing for a more suitable growth rate of tetrahedral cells. There is a prism boundary layer mesh at the wall of the spinner which has a near-wall Y+ of order one and an expansion rate of around 1.1. The spinner wall is viscous and rotating. A tetrahedral-based volume mesh is generated with a global expansion rate no greater than 1.05.

Figure 2(c) shows a cross-section view of the hybrid mesh approach. The global domain is the same geometric size in all three approaches. The hybrid approach mesh has a total of around 73 million cells, making it the smallest case in terms of computational demand. In comparison to the full-span approach, around 35% mesh saving is demonstrated. In addition, very high aspect ratio cells near the spinner associated with a fully structured mesh topology are avoided using the hybrid mesh strategy, which is potentially beneficial for numerical convergence.

VI. Results

A. Flow Distortion/Steady Flow Field

The intake geometry used in the present study is axisymmetric and, as a result, the flow distortion introduced is purely due to the non-zero inflow angle of attack (AoA). The flow distortion presented in this study includes the necessary physical mechanisms to evaluate the methodologies for the propagation of tonal noise through steady distorted flow.

The acceleration of flow around the bottom lip of the nacelle causes a circumferential inhomogeneity at the entry to

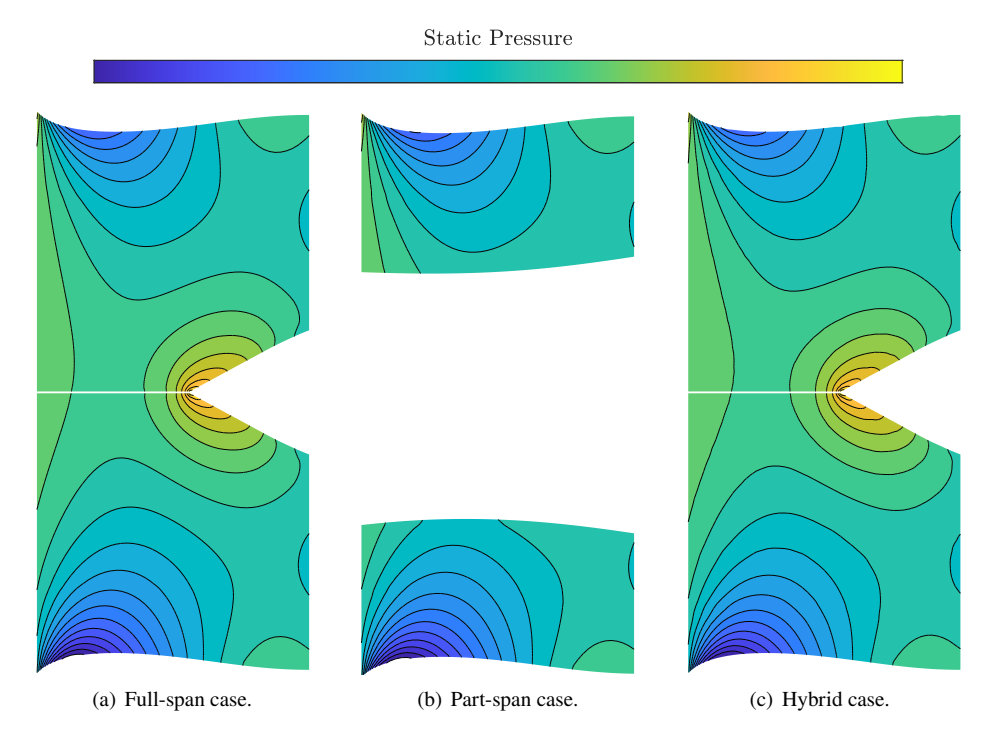


Fig. 3 A cross-section view of the time-averaged static pressure for each case, highlighting a side-on view of the top and bottom lip of the nacelle.

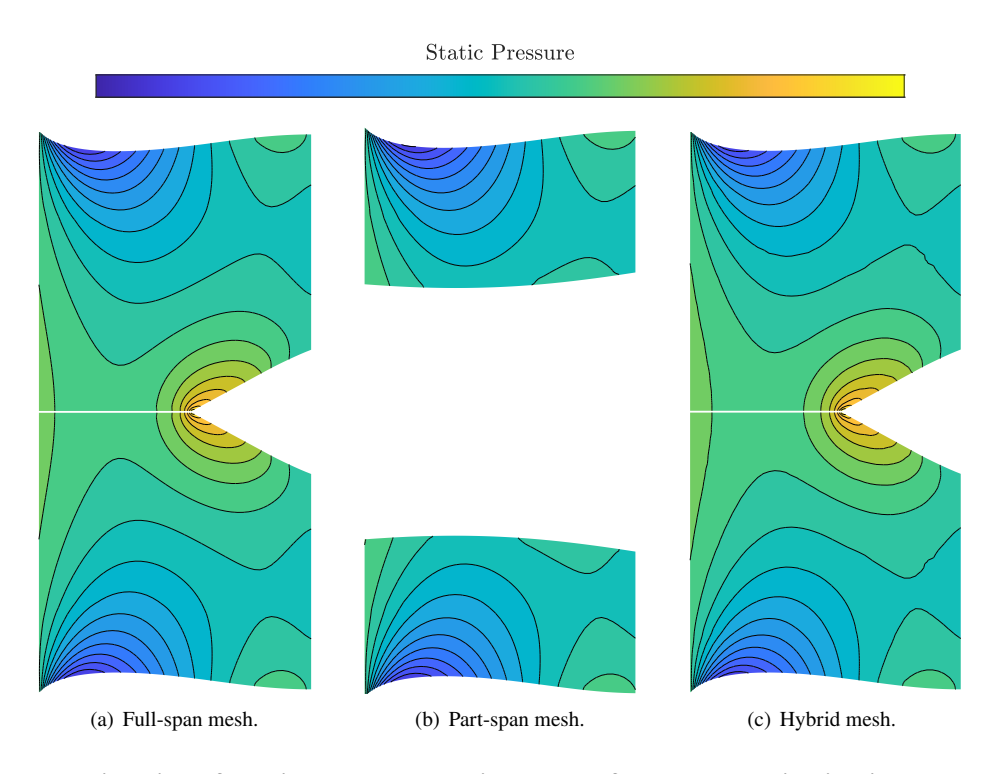


Fig. 4 A cross-section view of the time-averaged static pressure for each case, highlighting a top-down view of the nacelle.

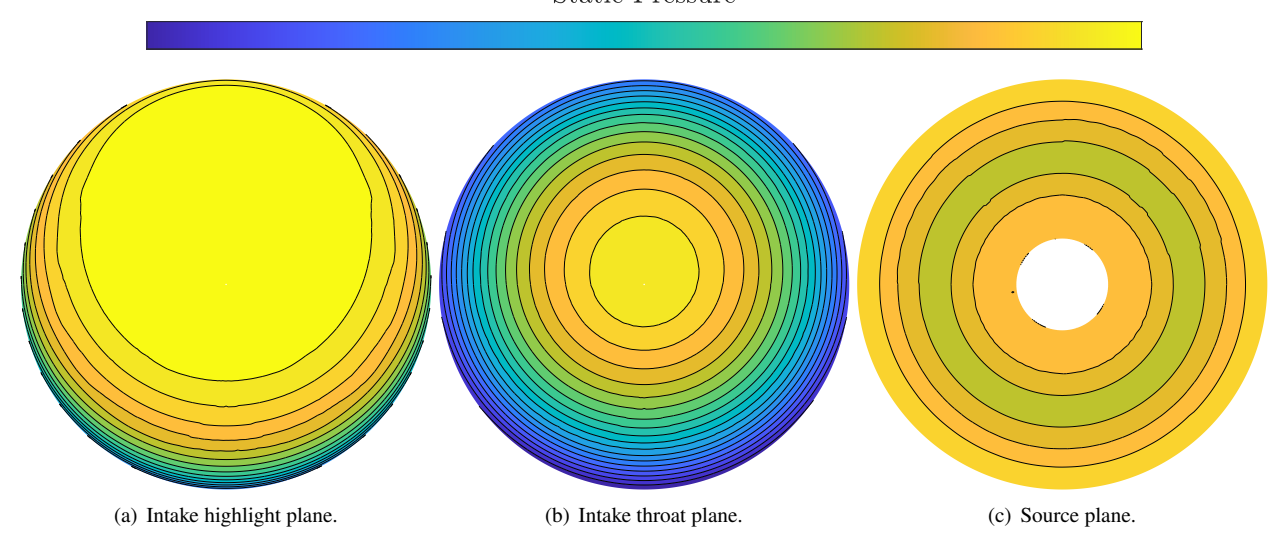


Fig. 5 Time-averaged static pressure at three different axial positions in the intake.

the intake. This distortion is primarily steady and potential, and the distortion level decreases as the flow approaches the source plane, as is later shown.

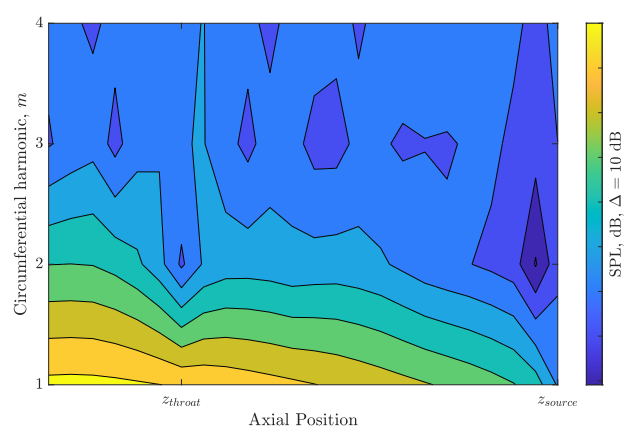
To explore the suitability of each meshing approach, the time-averaged flow is considered for each case. Figures 3 and 4 show cross sections of the time-averaged static pressure in the intake duct for each simulation result. The side-on view (Figure 3) highlights how the flow is asymmetrically accelerated in the duct, with a region of lower pressure at the bottom lip due to a greater acceleration at this point. The top-down view of the intake mean pressure field (Figure 4) highlights a more symmetric flow characteristic. Between each case, there are no significant/notable differences in the time-averaged flow which suggest that the distorted flow field is not impacted by each meshing philosophy. This was expected due to the low-frequency nature of this time-averaged flow. Furthermore, the use of a streamtube in the part-span case ensured that there was minimal impact on the flow due to the artificial boundary.

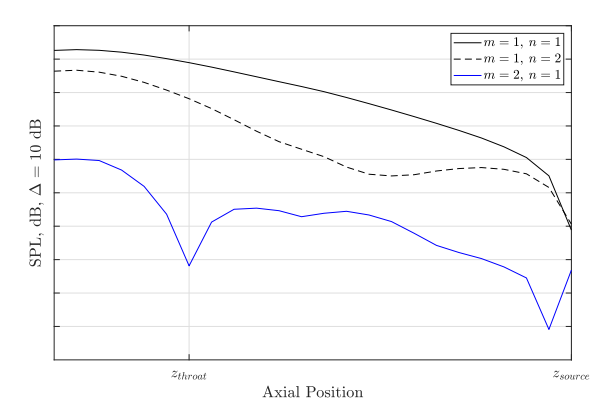
The time-averaged flow from the hybrid mesh case is now further considered to better evaluate the flow distortion in the duct. Figure 5 highlights the time-averaged static pressure at three different axial positions in the intake. At the most downstream position, the source plane (Figure 5(c)), the time-averaged flow field is axisymmetric. As the source itself doesn't include any presence of distortion, this is to be expected. The most significant circumferential inhomogeneity is observed at the intake highlight plane. By the intake throat position, there is still a notable circumferential variation in the duct. Locally, this plane has the lowest time-averaged pressure as the flow is accelerated to it's highest mean velocity in the duct at this position.

A number of studies [6, 7, 12, 16] have described inflow distortion by low-order azimuthal variations. In the present case, a Fourier-Bessel decomposition of the steady flow field in the intake was completed. Figure 6(a) highlights the amplitude of the first five azimuthal harmonics at the first radial harmonic along the intake. Figure 6(b) tracks the amplitude of the first azimuthal harmonic (m = 1) at the first and second radial harmonics through the intake. The amplitude of the second azimuthal mode is also plotted and is more than 25 dB lower than the components of the first azimuthal mode. Hence, the flow field can be mostly described by the first azimuthal mode component. Visible in both plots of Figure 6 is how the amplitude of the azimuthal variation decreases towards the source position. This observation is consistent with the expected behaviour of a decaying steady potential field.

There is a notable drop in the amplitude of the first azimuthal mode component (m = 1) at the most downstream axial position which appears to decay in an unphysical manner. This is due to the prescribed zero distortion at the source plane. In a coupled simulation, this plot highlights that there would still be a low level of distortion at this point. Nevertheless, the amplitude of this azimuthal component is still considerably lower (> 40 dB) than the peak level in the intake and is not considered substantial, confirming the findings of Wu and Wilson [16].

At the second radial mode, there is a dip in amplitude at the throat position. This is potentially due to a change in cut-off/cut-on ratio at this position, or due to radial mode interference. Given it's low amplitude with respect to the first azimuthal component, it is not further explored in the present study.





- (a) Azimuthal components of the steady flow field at the first radial harmonic along the intake.
- (b) Amplitude of isolated modal components of the steady flow field along the intake.

Fig. 6 Description of the steady distorted flow field in terms of Fourier-Bessel harmonics.

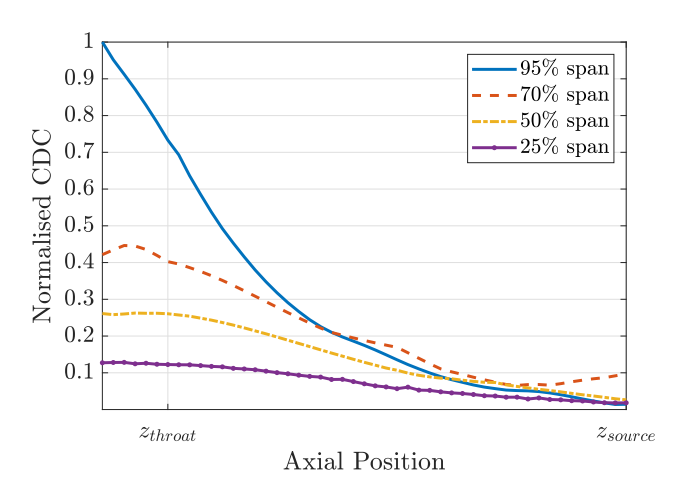


Fig. 7 Normalised CDC plotted against axial position at four spanwise positions.

Previous studies, [14, 50, 53, 54] for example, have defined parameters to describe the distorted field in an aeroengine duct. For complex distorted fields, some parameters can lack the detail required to convincingly describe the distortion. However, when the distorted field is relatively simple, as is the present case, such parameters can be useful for visualising the distortion level. Daroukh et al. [14] introduced the Circumferential Distortion Coefficient (CDC),

$$CDC(x, h/H) = \frac{\operatorname{Max}_{\theta}[M(z, h/H, \theta)] - \operatorname{Min}_{\theta}[M(z, h/H, \theta)]}{\operatorname{Mean}_{\theta}[M(z, h/H, \theta)]},$$
(1)

where $M(z, h/H, \theta)$ is time-averaged Mach number. The CDC considers the azimuthal deviation of the temporally averaged flow in comparison to the circumferentially averaged flow profile at each axial and spanwise position. Figure 7 presents the normalised value of CDC along the intake duct at four spanwise positions for the present study. At all spanwise positions, the level of distortion is higher towards the upstream end of the intake, and this level decreases to a low level towards the source. The highest level is observed for the highest spanwise position (95%), and this gradually decreases as the span decreases. This description of the distorted field suggests that the greatest impact of distortion on the acoustic field will be at the upstream region of the intake. This is further explored when the acoustic field is discussed.

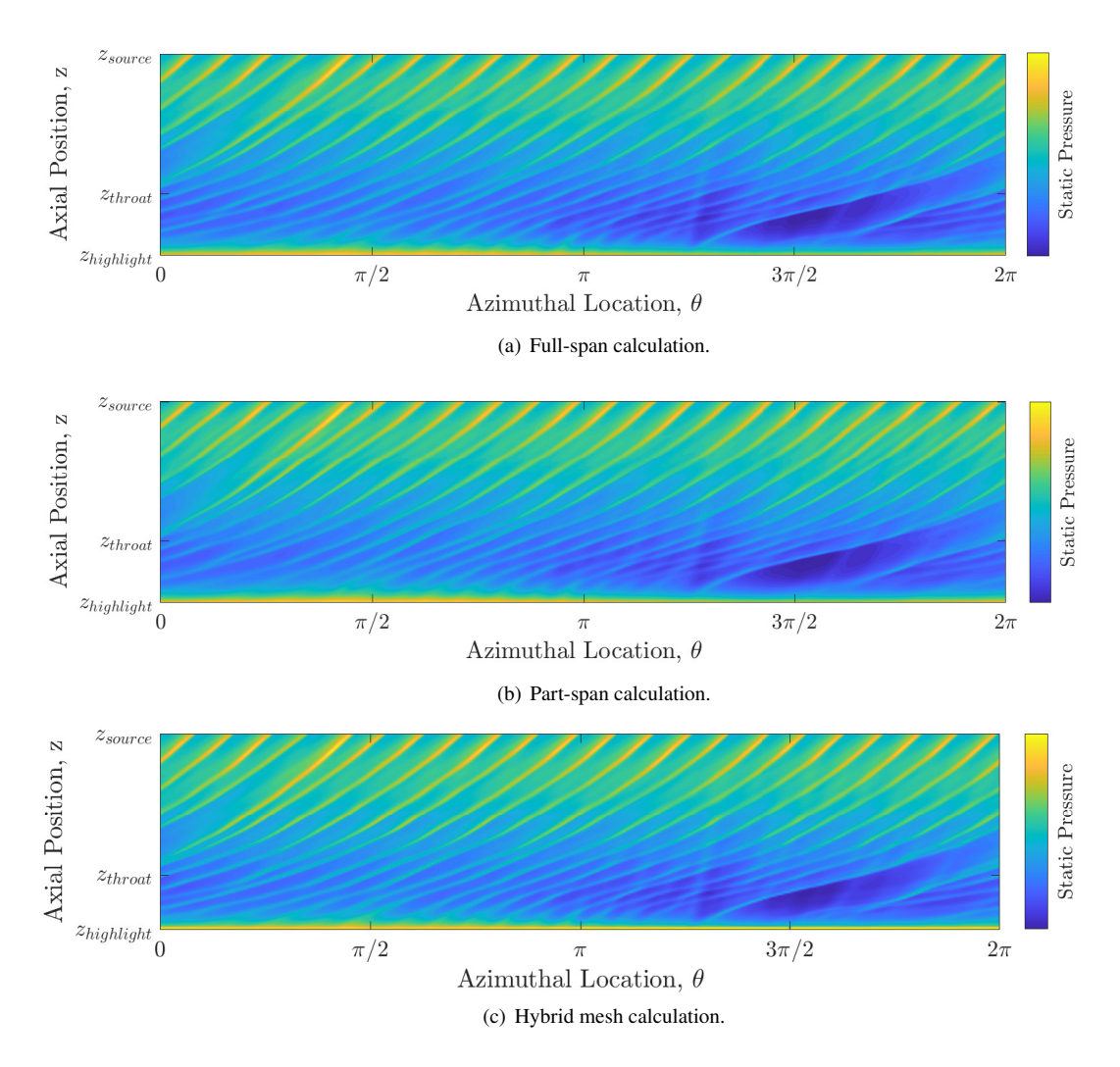


Fig. 8 Instantaneous static pressure contour plots showing the propagation of the shock field on the intake duct outer wall from the source position up to the highlight for each calculation. The top of the nacelle corresponds to an azimuthal position of $\theta = 0$ and the bottom of the nacelle corresponds to an azimuthal position of $\theta = 3\pi/2$.

B. Instantaneous Flow Field

This section will briefly consider the instantaneous flow field of the converged solution in the intake duct for results from each meshing approach. Figure 8 shows the static pressure on the nacelle wall through the intake duct for each calculation. Between the three cases, there is little variation in the observed pressure field on the nacelle wall. The axial dissipation of the shockwaves through the intake is similar in each case. Our previous work [20], which considered a full-span and part-span approach for the same case, but computed in different numerical solvers, showed a notable difference in shockwave decay between the cases and highlights the relevance of the present study.

Other propagation effects can also be identified in these contours. For example, the impact of the distorted field on the propagation of the tonal field which seems to be significantly modified. This is most notable at the bottom lip of the nacelle ($\theta = 3\pi/2$) where the region of high axial velocity causes a turning of the shock field direction during propagation.

The significance of a non-uniform blade stagger angle in the source can also be highlighted by the initial variation of the shock-to-shock propagation angle and how this varies from peak-to-peak through the intake, causing the peaks in pressure to be positioned at varying distances at different axial positions.

C. Acoustic Field

The following section considers the acoustic field in the intake at the first two Blade Passing Frequencies (BPFs). This data was obtained by completing a temporal Fourier transform for each case over a full revolution at every point through the domain. The Fourier amplitudes at these frequencies are used in the following analysis.

Multiple effects can be observed during the propagation of shock-associated noise through the intake. The first is non-linear decay due to the high amplitude of shock-associated noise. This effect would be observed for a uniformly staggered fan source and a mean field without distortion. When a fan source with non-uniform stagger variation is considered, as is the case here, the non-uniform shock field causes redistribution of acoustic energy between different engine orders during propagation. This effect would be observed for a case with no flow distortion and has been considered by other studies ([31, 33, 42]). The final effect is due to the acoustic field's interaction with the steady flow distortion in the intake. As was introduced during the literature review, studies have considered the impact of flow distortion on the acoustic field in an aeroengine. This effect has been observed independently of blade stagger variation [11] and non-linearity effects [50]. In reality, and in the present study, a combination of these effects occur and are significant to the evolution of the acoustic field.

Figure 9 presents the distribution of Sound Pressure Level (SPL) on the outer wall of the duct at the first BPF for each case. Most deviation from the datum case is observed in the part-span case, with a significant difference toward the upper lip of the nacelle ($\theta = 0$). The lowest amplitude at this frequency in all cases is observed at the bottom lip of the intake ($\theta = 3\pi/2$) due to the greater acceleration of flow at this point, as previously discussed. The amplitude distribution in both the full-span and hybrid mesh cases is similar. There are minor differences in some of the finer details of the amplitude at different locations. Throughout the duct, there are some strips of reduced amplitude observed in all cases. Wu and Wilson [16] demonstrated for an undistorted case that this is due to interference between different radial harmonics during propagation. This effect may appear significant, but may be the result of the interaction of components with high amplitude close to the cut-off/cut-on boundary, which is highlighted in Figure 10(a) and discussed in the following paragraph. Consequently, the impact in the far field may be minimal, as later discussed. It was not expected that the part-span case could accurately resolve this radial interference due to the difference in duct geometry. For the most part, the greater dips in amplitude are resolved in all cases. The bigger differences in the part-span case upstream of the throat may be due to this radial mode interference effect.

To observe the impact of distortion, an azimuthal mode distribution at the first BPF of the acoustic field obtained by the hybrid mesh case is presented in Figure 10. Figure 10(a) presents a contour of the amplitude of different azimuthal components (at the first radial mode) during propagation. Approximations for the cut-off/cut-on ratio are also presented by the black and red lines, which are based on the mean flow across the whole span and 90% span, respectively, as well as an annular duct assumption at each axial position. Figure 10(b) shows the amplitude of the rotor-locked 1 BPF acoustic mode (m = 22) and the neighbouring azimuthal components during propagation. At the downstream region of the intake, the m = 22 azimuthal component dominates more than 25 dB higher than any other components. During propagation, the amplitude decays up to the throat where the neighbouring modes have comparable amplitude. Figure 10(a) highlights that the most significant mode scattering occurs in the upstream half of the intake. This coincides with how the level of distortion varies through the intake, as previously observed (Section VI.A).

As well as mode scattering to directly neighbouring azimuthal components, a peak is also observed at higher azimuthal components ($m \approx 26$) and coincides with the cut-off/cut-on ratio approximations. Modes close to the cut-off/cut-on boundary typically have high amplitude but carry little acoustic power and so may not be important. The approximations for this boundary consider the axial Mach number across the whole span (black) and at 90% span (red). The 90% span approximation is more relevant here as more of the acoustic energy is positioned towards the outer radius.

To compare between each case, the azimuthal mode distribution at the first radial mode and first BPF is compared at the throat axial position in Figure 11. At the source plane, the mode decomposition is the same as all cases use the same source. There were some small, considered negligible, differences observed in the part-span case at the source position due to the change in domain size. Following propagation upstream to the throat, the extent of mode scattering is evident by the increase in amplitude of all neighbouring modes. All methodologies resolve the highest amplitude components reasonably. At the m = 21 component, the part-span approach underpredicts the component amplitude by around 4 dB. The hybrid case aligns with the baseline to within 1 dB for the two neighbouring upstream and downstream components. Away from this, some small deviations are apparent, but are less significant as they have much lower amplitude.

Figure 12 shows the distribution of SPL at the second BPF on the outer wall of the intake duct for each case. The highest amplitude is observed at the source, and the amplitude decays through the intake. Similarly to the amplitude distribution at the first BPF, for all cases, the lowest amplitude is observed at the lower lip of the intake $(3\pi/2)$. For the part-span case, the amplitude decays more significantly in the upstream region of the intake in comparison to the other

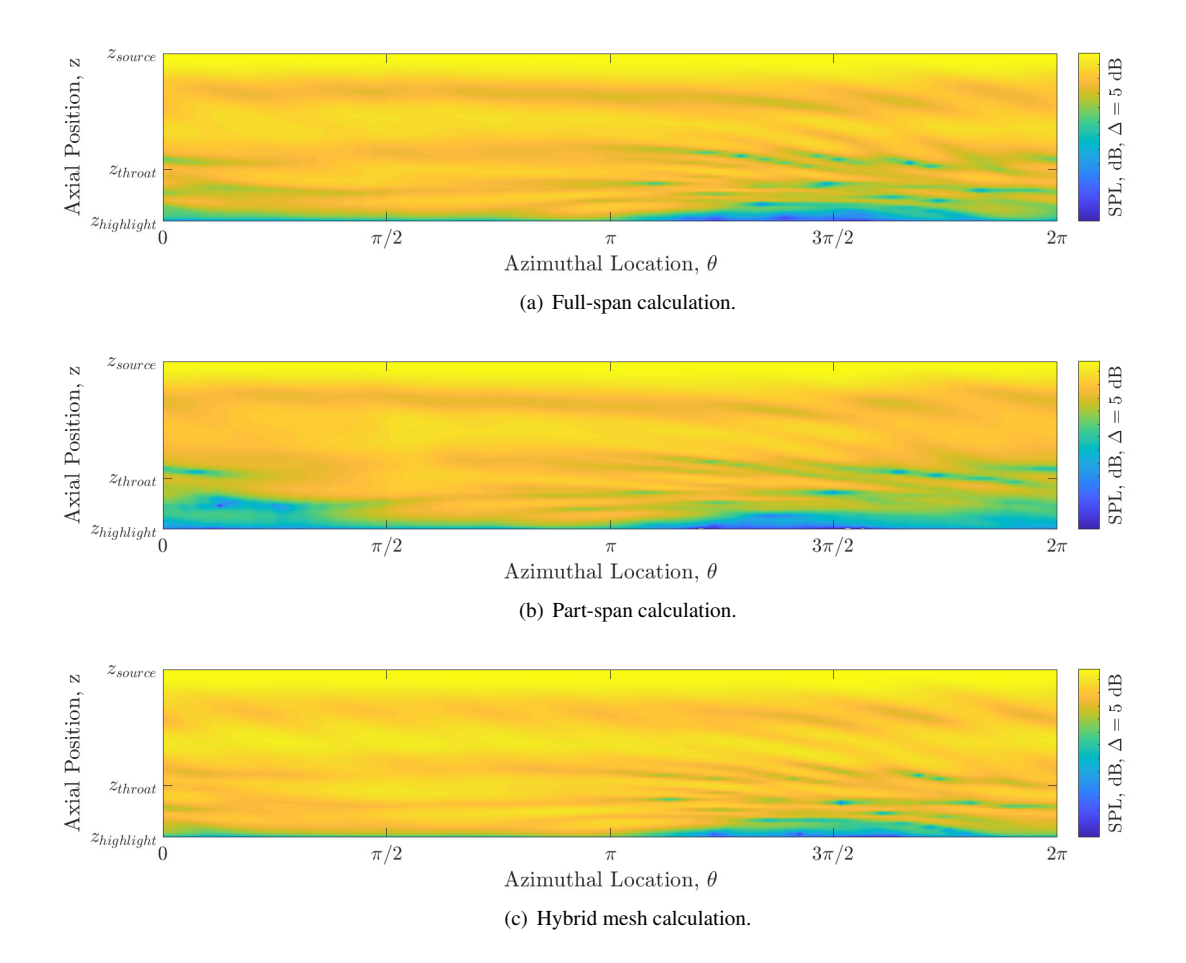
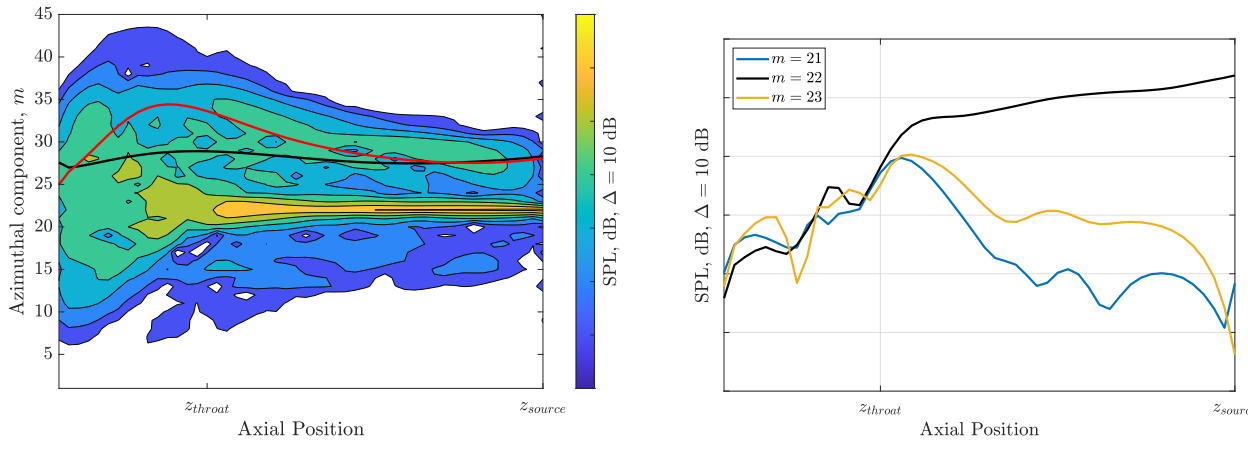


Fig. 9 Distribution of Sound Pressure Level (SPL) at 1BPF on the outer wall of the duct for each case.



(a) Contour plot showing the amplitude evolution of different azimuthal components through the intake. The black line (–) is an approximation of the cut-off/cut-on ratio based on the average Mach number at each axial position. The red line (–) is the same approximation but based on the average Mach number at 90% span at each axial position.

(b) Evolution of the amplitude of the rotor-locked 1BPF acoustic mode (m = 22) and two neighbouring modes.

Fig. 10 Azimuthal mode distribution at the first BPF. Both plots correspond to only the first radial harmonic and are plotted for the hybrid mesh case only.

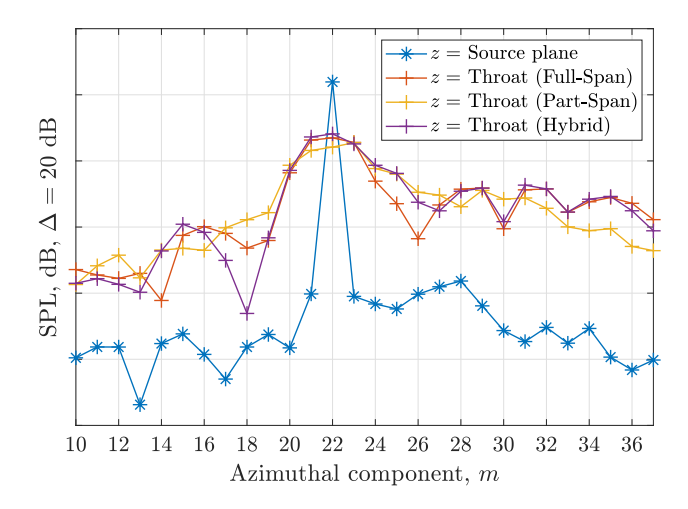


Fig. 11 The azimuthal mode distribution at the first radial mode and the first BPF computed at the throat axial position for each simulation.

simulations. An azimuthal mode distribution at the second BPF and throat axial position is presented in Figure 13(a) for each case. This comparison highlights some potentially significant differences, particularly for the part-span approach. As for the first BPF, at the source plane, only one case is shown as negligible variations are observed. After propagation to the throat, the amplitude of the rotor-locked mode at the second BPF (m = 44) has decayed by around 15 dB and is comparable with neighbouring modes that have significantly increased in amplitude. In fact, the amplitude of this mode is lower than azimuthal components from m = 46 to m = 48. It was suspected that this was due to the location of cut-off/cut-on ratio, though this value is predicted to be higher than these peak azimuthal positions at the throat, as is highlighted in Figure 13(b) which considers the azimuthal mode distribution through the duct for the hybrid mesh case. The high amplitudes at these circumferential orders are potentially due to the non-linear interaction between the rotor-locked 1 BPF mode (m = 22) and the high-amplitude components observed near the cut-off/cut-on boundary at 1 BPF (highlighted in Figure 10(a)). As observed at 1 BPF, most significant mode variation occurs around the throat axial position and upstream of it, as the amplitude of the peak significantly decays.

VII. Summary & Discussion

The part-span and hybrid computational methodologies presented in this study achieve significant computational savings while resolving the majority of the acoustic field of interest. Both methods successfully captured high-amplitude acoustic content at the first blade passing frequency (BPF). However, at the second BPF, the part-span approximation struggled to resolve the acoustic field in the upstream half of the intake, while the hybrid approach effectively resolved both the general distribution of sound pressure level and the dominant azimuthal mode components.

This study employed a decoupled approach, propagating an undistorted source through the intake. In some cases, this may be beneficial, such as when only propagation effects are concerned, or the effectiveness of a liner are considered. However, coupled simulations resolving both source and propagation mechanisms are sometimes preferred, particularly for cases with high-distortion levels cases.

To address this, two solutions are proposed. The first is to use a hybrid meshing approach, as introduced in the present study, coupled to a typical fully structured high-quality fan stage mesh. With the current hybrid intake mesh, this would achieve around a 20% computational saving, applying a fan stage mesh such as the one presented by Wu and Wilson [16]. As mentioned in Section IX, further development of the hybrid mesh in the intake is anticipated to further increase the available computational saving using such approach.

The second proposed solution is a two-part source-propagation calculation. The source calculation would encompass the whole computational domain but only resolve the acoustic field in the fan domain. The intake domain would have a mesh fine enough to capture the flow field and any potential flow distortion, but too coarse to propagate the acoustic content through the duct. For the propagation calculation, the intake would be considered separately using a high-resolution mesh sufficient to resolve the acoustic field. The steady and unsteady components of the pressure profile at the fan face would be extracted from the prior source calculation and used as an input for the propagation calculation

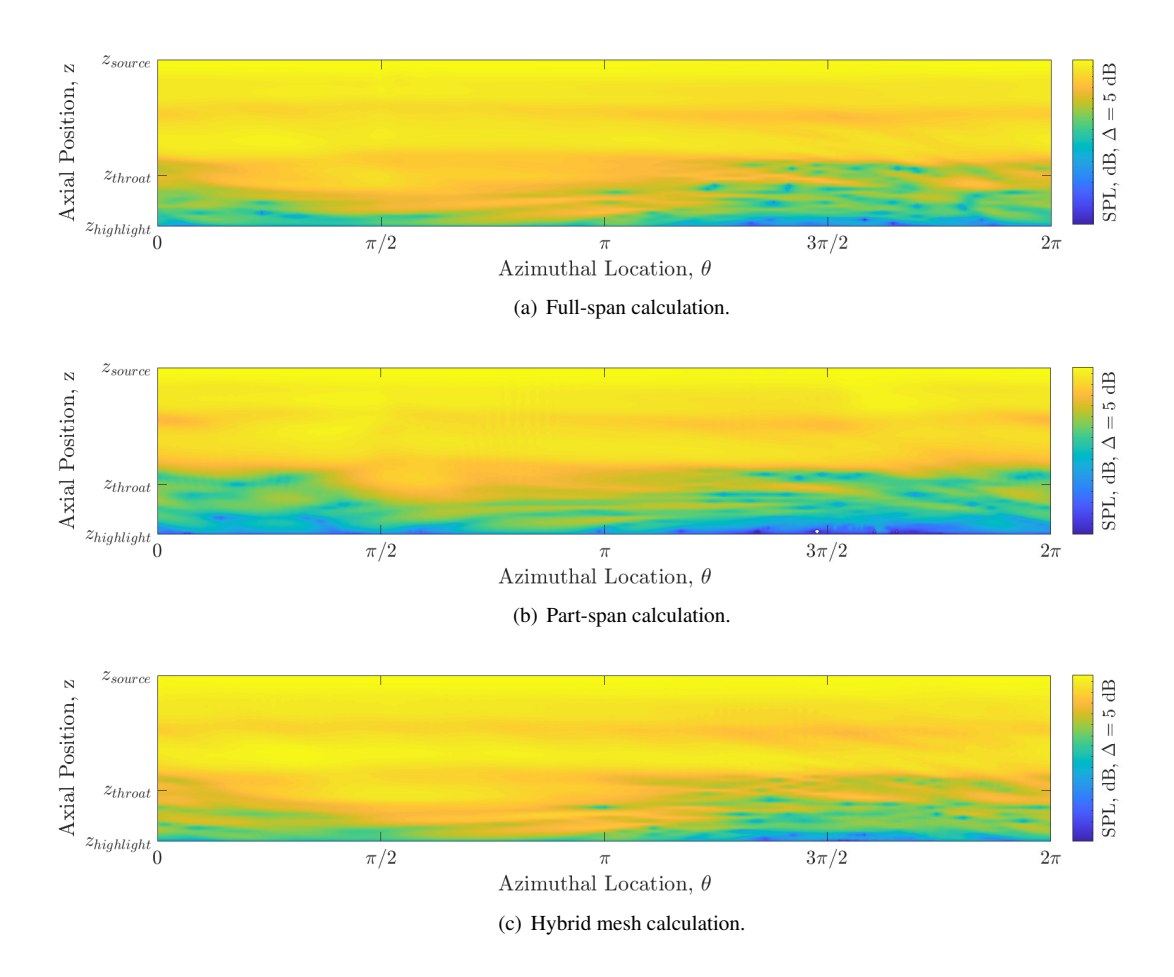


Fig. 12 Distribution of Sound Pressure Level (SPL) at 2BPF on the outer wall of the duct.

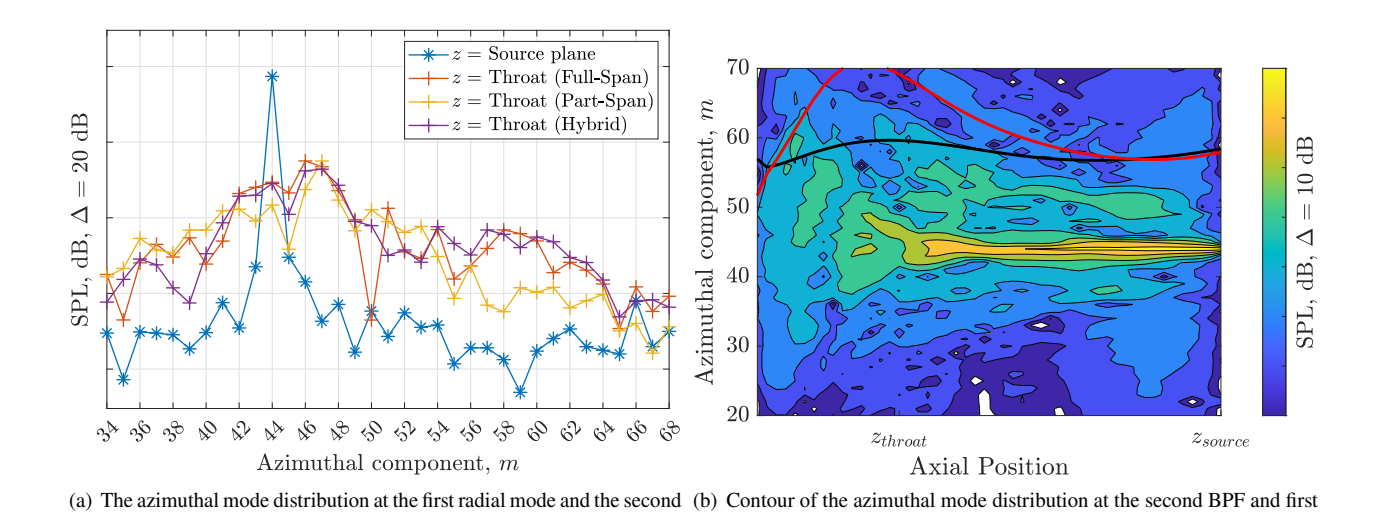


Fig. 13 Azimuthal mode distribution at the second BPF. Both plots correspond to only the first radial harmonic.

radial mode through the intake.

BPF computed at the throat axial position for each simulation.

applying the same methodology as that used in the present work.

This two-part method offers significant savings as the domain becomes effectively shorter and the mesh count is smaller in both calculations. In the source calculation, the time to convergence is reduced because acoustic content no longer has to propagate upstream through the intake duct. In the propagation calculation, the fan is not considered, significantly reducing the mesh count. The suggested mesh approach taken for the propagation calculation would be a hybrid mesh due to it's performance in resolving the acoustic field and high computational saving. For the current case, a two-part source-propagation calculation using a hybrid mesh for the propagation calculation is expected to achieve a computational saving of around 65%, and up to 70% with an optimised hybrid intake mesh (Section IX).

Alongside validation of each methodology, the acoustic field at the first two BPFs was considered. At both frequencies, rotor-locked acoustic modes (m = nB) dominate in the first stage of propagation. Consistent with the distortion evolution through the duct, the most pronounced mode scattering occurs in the upstream half of the duct. By the time the tone noise has propagated upstream of the intake throat, the acoustic field at both frequencies is no longer described by the rotor-locked acoustic modes and many more azimuthal modes become significant. At the first BPF, these components are mostly close to the rotor-locked mode, though at the second BPF, a broader range of azimuthal modes are relevant and are required to describe the acoustic field at this point. This mode scattering effect will likely be more significant for shorter intake designs where the level of distortion is anticipated to be higher, and have high amplitude at the source. Of particular practical consequence may be the potential effect on acoustic liner effectiveness when scattering occurs near the location of the liner. In the current case, the impact would be minimal as most significant scattering occurs upstream of the acoustic liner position, though this may not be true for cases with greater distortion levels at downstream regions of the intake.

VIII. Conclusions

The present study has considered three computational approaches for URANS CFD predictions of high-amplitude shock-associated tone noise propagation through an aeroengine intake with steady flow distortion.

The datum case followed a conventional fully structured mesh approach, as has been validated in other previous studies [9, 16].

The second applied a part-span approximation, a methodology that we have previously introduced [19, 20], that neglects low span regions of the duct according to the observation that most of the acoustic energy flux in the duct is concentrated towards the outer walls. This mesh was also fully structured, with the same resolution as the datum case in the region that was discretised and offered a computational saving of around 30%.

The final case implemented a hybrid meshing approach, combining a structured mesh region at high-span regions in the duct, a semi-structured h-block in the intake which varied azimuthal resolution with radius, and an unstructured region at low-span regions and in the far-field. This approach offered the greatest computational saving ($\tilde{3}5\%$) and discretized the whole domain. Use in conjunction with a two-part source-propagation calculation (outlined in the previous section), a complete prediction could be achieved with an anticipated computational saving of around 70%.

The time-averaged unsteady flow, instantaneous pressure field and acoustic fields were considered for each case.

The time-averaged unsteady flow highlighted the steady flow distortion in the intake duct which was found to be sufficiently resolved by each case. The flow distortion was described in terms of low-order azimuthal components as well as by considering the azimuthal variation in the flow at different azimuthal and radial positions according to a definition introduced by Daroukh et al. [14]. The distortion level was highest at the upstream entry to the intake and decayed as a steady potential field towards the source plane.

The instantaneous pressure field highlighted the propagation and decay of the shock field through the intake. The variation in shock strength due to the buzz-saw noise source was evident and could be resolved in each case. The axial dissipation of the shock field was observed to be similar in each case.

The acoustic field at the first and second BPF was considered for each case. The hybrid mesh approach resolved the highest peaks at both BPFs to within 2 dB. the part-span mesh case could resolve these peaks to within 5 dB. On the duct outer wall, minimal variations in SPL at the first to BPFs were observed in the hybrid case. Some deviations were observed for the part-span case, particularly at the top lip of the intake ($\theta \approx 0$), where a lower amplitude was apparent at both BPF's. Toward the upstream end of the intake, the part-span case predicted a lower amplitude at the second BPF, which could be significant.

To reduce the computational expense of this type of simulation, the hybrid mesh approach was determined to be most suitable, offering a significant computational saving and sufficiently resolving the distorted flow field and acoustic field at the frequencies considered in the present study.

Following this conclusion, the impact of steady flow distortion on the acoustic field was considered, mainly using the data from the hybrid mesh case. The acoustic field at the first two BPF's were decomposed into their Fourier-Bessel acoustic modes. Azimuthal mode distributions were then considered at both frequencies. Acoustic mode scattering was observed in the upstream half of the intake where the flow distortion level was highest. At the first BPF, mode scattering was most significant for the azimuthal components directly next to the rotor-locked mode. Peaks were also observed at circumferential orders close to the cut-off/cut-on boundary. At the second BPF, significant mode scattering effect seemed to occur upstream of the throat position into azimuthal components higher than the rotor-locked 2BPF mode.

IX. Future work

Areas of future work identified during this study include:

- Fourier-Bessel wavesplitting analysis, such as that presented by Wu and Wilson [16], to understand the upstreamand downstream-travelling waves in the intake. This would allow for a better description of the acoustic and distorted flow fields, as well as increasing the understanding of the distortion effects observed in the present study.
- A full 3D modal breakdown of the acoustic field, and comparison of this with the present Fourier-Bessel decomposition may offer increased understanding of the impact of distortion.
- Consideration of the acoustic field at all of the frequencies corresponding to the full buzz-saw spectrum (in the present case, for frequencies relating to EO 1-22). Given the multitude of complex effects present in the intake (non-linearity, shock-to-shock variations in the buzz-saw noise field, and the interaction of the acoustic and distorted fields), analysing more of the acoustic field may allow for a more detailed separation of each effect.
- Extension of the hybrid methodology presented in the current study. The present hybrid mesh used a streamtube to define the interface to the unstructured mesh region. To make the mesh more general, and easier to apply, a more general interface is suggested at a percentage of the span position. It is also proposed to optimise the azimuthal resolution of the semi-structured region according to the amount of acoustic energy present in the intake which could be informed by our previous linear propagation work [19]. It is anticipated that this would further reduce the mesh count in the intake leading to further savings in computational cost.
- Implementation of the two-part source-propagation method introduced and explained in Section VII
- Only a shallow in-flight angle of attack was considered, leading to a relatively low distortion level. There is
 significant interest in applying the current methodologies for cases with more significant distortion levels due to
 both flight conditions and the inclusion of more realistic, drooped three-dimensional intake geometries.

Acknowledgments

The work presented in this paper is funded through the PhD work of the first author which is financially supported by the University of Southampton and Rolls-Royce plc. The second and third authors acknowledge funding support from the Innovate UK Research Programme FANTASIA - Future Aircraft Noise Technologies And Systems Integration Analytics (ref. 74217). The authors wish to acknowledge Howoong Namgoong, the wider noise team and the CFD team at Rolls-Royce for their continued support and technical discussion. Rolls-Royce are also acknowledged for data provided throughout this project. The authors acknowledge the use of the IRIDIS High Performance Computing Facility, and associated support services at the University of Southampton.

References

- [1] European Commission. Directorate-General for Mobility and Transport. Directorate-General for Research and Innovation., Flightpath 2050: Europe's vision for aviation: maintaining global leadership and serving society's needs., 2011. https://doi.org/10.2777/50266.
- [2] UK-Civil-Aviation-Authority, "Aviation noise and health; the effects of aviation noise,", 2023. URL https://www.caa.co.uk/consumers/environment/noise/aviation-noise-and-health/, accessed on 12/05/2023.
- [3] Moreau, S., "Turbomachinery Noise Predictions: Present and Future," *Acoustics*, Vol. 1, No. 1, 2019, pp. 92–116. https://doi.org/10.3390/acoustics1010008.
- [4] "Rolls-Royce UltraFan,", 2024. URL https://www.rolls-royce.com/innovation/ultrafan.aspx.
- [5] Carnevale, M., Wang, F., and Mare, L. D., "Low Frequency Distortion in Civil Aero-engine Intake," *Journal of Engineering for Gas Turbines and Power*, Vol. 139, No. 4, 2017. https://doi.org/10.1115/1.4034600.

- [6] Schwaller, P. J., Tester, B. J., and Henshaw, D. G., "The effects on fan noise of inlet steady flow distortion," 3rd AIAA/CEAS Aeroacoustics Conference, 1997, pp. 40–46. https://doi.org/10.2514/6.1997-1590.
- [7] Schwaller, P. G., Baker, N. J., Tomlinson, J. D., Sijtsma, P., and Hemmings, R., "Noise validation of model fan rig with engine," *Collection of Technical Papers 12th AIAA/CEAS Aeroacoustics Conference*, Vol. 2, No. May, 2006, pp. 1014–1025. https://doi.org/10.2514/6.2006-2479.
- [8] Astley, R. J., Sugimoto, R., and Mustafi, P., "Computational aero-acoustics for fan duct propagation and radiation. Current status and application to turbofan liner optimisation," *Journal of Sound and Vibration*, Vol. 330, No. 16, 2011, pp. 3832–3845. https://doi.org/10.1016/j.jsv.2011.03.022, URL http://dx.doi.org/10.1016/j.jsv.2011.03.022.
- [9] Doherty, M., and Namgoong, H., "Impact of turbofan intake distortion on fan noise propagation and generation," 22nd AIAA/CEAS Aeroacoustics Conference, 2016, 2016, pp. 1–18. https://doi.org/10.2514/6.2016-2841, URL http://dx.doi.org/10.2514/6.2016-2841.
- [10] Prinn, A. G., Sugimoto, R., and Jeremy Astley, R. J., "The effect of steady flow distortion on noise propagation in turbofan intakes," 22nd AIAA/CEAS Aeroacoustics Conference, 2016, 2016, pp. 1–14. https://doi.org/10.2514/6.2016-3028.
- [11] Daroukh, M., Moreau, S., Gourdain, N., Boussuge, J. F., and Sensiau, C., "Influence of distortion on fan tonal noise," 22nd AIAA/CEAS Aeroacoustics Conference, 2016, 2016.
- [12] Winkler, J., Reimann, C. A., Gumke, C. D., Ali, A. A., and Reba, R. A., "Inlet and aft tonal noise predictions of a full-scale turbofan engine with bifurcation and inlet distortion," 23rd AIAA/CEAS Aeroacoustics Conference, 2017, 2017, pp. 1–14. https://doi.org/10.2514/6.2017-3034.
- [13] Daroukh, M., "Effect of distortion on modern turbofan tonal noise," Ph.D. thesis, Université de Toulouse, 2017. URL https://theses.hal.science/tel-04222919v1/file/DAROUKH_Majd.pdf.
- [14] Daroukh, M., Moreau, S., Gourdain, N., Boussuge, J. F., and Sensiau, C., "Tonal noise prediction of a modern turbofan engine with large upstream and downstream distortion," *Journal of Turbomachinery*, Vol. 141, No. 2, 2019. https://doi.org/10.1115/1. 4042163.
- [15] Daroukh, M., Polacsek, C., and Chelius, A., "Shock wave generation and radiation from a turbofan engine under flow distortion," AIAA Journal, Vol. 58, No. 2, 2020, pp. 787–801. https://doi.org/10.2514/1.J058799, URL https://doi.org/10.2514/1.J058799.
- [16] Wu, L., and Wilson, A. G., "Fan Buzz-Saw Noise under Intake Flow Distortion: a Computational Study," 30th AIAA/CEAS Aeroacoustics Conference, 2024, 2024.
- [17] McAlpine, A., and Fisher, M. J., "On the prediction of "buzz-saw" noise in aero-engine inlet ducts," *Journal of Sound and Vibration*, Vol. 248, No. 1, 2001, pp. 123–149. https://doi.org/10.1006/jsvi.2001.3770.
- [18] Stratford, B., and Newby, D., "A New Look at the Generation of Buzz-saw Noise," 44th AIAA Aeroacoustics Conference, 1977, pp. 1–23. https://doi.org/10.2514/6.1977-1343.
- [19] Binns, J. S. P., Wu, L., and Wilson, A. G., "Part-Span Approximation of Tone Noise Propagation in an Aeroengine Intake. Part I: Linear Propagation," 30th AIAA/CEAS Aeroacoustics Conference, 2024, 2024.
- [20] Binns, J. S. P., Wu, L., and Wilson, A. G., "Part-Span Approximation of Tone Noise Propagation in an Aeroengine Intake. Part II: Non-Linear Propagation," 30th AIAA/CEAS Aeroacoustics Conference, 2024, 2024.
- [21] Sturm, M., Sanjose, M., Moreau, S., and Carolus, T., "Aeroacoustic simulation of an axial fan including the full test rig by using the lattice boltzmann method," *FAN 2015 International Conference on Fan Noise, Technology and Numerical Methods*, Vol. 2015-April, 2015, pp. 1–12.
- [22] Gonzalez-Martino, I., and Casalino, D., "Fan tonal and broadband noise simulations at transonic operating conditions using Lattice-Boltzmann methods," 2018 AIAA/CEAS Aeroacoustics Conference, 2018. https://doi.org/10.2514/6.2018-3919.
- [23] Casalino, D., Hazir, A., and Mann, A., "Turbofan Broadband Noise Prediction Using the Lattice Boltzmann Method," *AIAA Journal*, Vol. 56, No. 2, 2018, pp. 609–628. https://doi.org/10.2514/1.J055674.
- [24] Redonnet, S., Mincu, C., and Manoha, E., "Computational AeroAcoustics of Realistic Co-Axial Engines," *14th AIAA/CEAS Aeroacoustics Conference*, 2008.
- [25] Antwerpen, B. V., Leneveu, R., Caro, S., and Ferrante, P., "New advances in the use of Actran/TM for nacelle simulations," *14th AIAA/CEAS Aeroacoustics Conference*, 2008. URL www.fft.be.

- [26] Rarata, Z., Gabard, G., Sugimoto, R., Coupland, J., Astley, R. J., Namgoong, H., and Schwaller, P. J., "Integrating CFD source predictions with time-domain CAA for intake fan noise prediction," 20th AIAA/CEAS Aeroacoustics Conference, 2014, pp. 1–15. https://doi.org/10.2514/6.2014-2456.
- [27] Tam, C. K., and Webb, J. C., "Dispersion-relation-preserving finite difference schemes for computational acoustics,", 1993. https://doi.org/10.1006/jcph.1993.1142.
- [28] Ashcroft, G., and Zhang, X., "Optimized prefactored compact schemes," *Journal of Computational Physics*, Vol. 190, No. 2, 2003, pp. 459–477. https://doi.org/https://doi.org/10.1016/S0021-9991(03)00293-6, URL https://www.sciencedirect.com/science/article/pii/S0021999103002936.
- [29] Della Ratta Rinaldi, R., Iob, A., and Arina, R., "An efficient discontinuous Galerkin method for aeroacoustic propagation," *International Journal for Numerical Methods in Fluids*, Vol. 69, No. 9, 2012, pp. 1473–1495. https://doi.org/https://doi.org/10.1002/fld.2647, URL https://onlinelibrary.wiley.com/doi/abs/10.1002/fld.2647.
- [30] Morfey, C., and Fisher, M., "Shock-Wave Radiation From Supersonic Ducted Rotor," *Aeronautical Journal*, Vol. 74, No. 715, 1970, pp. 579–585. https://doi.org/10.1017/s0001924000049095.
- [31] Fisher, M. J., Tester, B. J., and Schwaller, P. J., "Supersonic fan tone noise prediction," 4th AIAA/CEAS Aeroacoustics Conference, 1998, pp. 290–300. https://doi.org/10.2514/6.1998-2249.
- [32] McAlpine, A., and Fisher, M. J., "On the prediction of "buzz-saw" noise in acoustically lined aero-engine inlet ducts," *Journal of Sound and Vibration*, Vol. 265, No. 1, 2003, pp. 175–200. https://doi.org/10.1016/S0022-460X(02)01446-3.
- [33] McAlpine, A., Fisher, M. J., and Tester, B. J., ""Buzz-saw" noise: A comparison of measurement with prediction," *Journal of Sound and Vibration*, Vol. 290, No. 3-5, 2006, pp. 1202–1233. https://doi.org/10.1016/j.jsv.2005.05.028.
- [34] McAlpine, A., Fisher, M. J., and Tester, B. J., ""Buzz-saw" noise: A comparison of modal measurements with an improved prediction method," *Journal of Sound and Vibration*, Vol. 306, No. 3-5, 2007, pp. 419–443. https://doi.org/10.1016/j.jsv.2007. 04.053.
- [35] McAlpine, A., Schwaller, P. J., Fisher, M. J., and Tester, B. J., "Buzz-saw noise: Prediction of the rotor-alone pressure field," *Journal of Sound and Vibration*, Vol. 331, No. 22, 2012, pp. 4901–4918. https://doi.org/10.1016/j.jsv.2012.06.009, URL http://dx.doi.org/10.1016/j.jsv.2012.06.009.
- [36] Tyler, J. M., and Sofrin, T. G., "Axial flow compressor noise studies," SAE Technical Paper 620532, 1962. https://doi.org/10.4271/620532.
- [37] Rienstra, S. W., "Sound transmission in slowly varying circular and annular lined ducts with flow," *Journal of Fluid Mechanics*, Vol. 380, 1999, p. 279–296. https://doi.org/10.1017/S0022112098003607.
- [38] Wilson, A. G., "Propagation of acoustic perturbations in non-uniform ducts with non-uniform mean flow using eigen analysis in general curvilinear coordinate systems," *Journal of Sound and Vibration*, Vol. 443, 2019, pp. 605–636. https://doi.org/10.1016/j.jsv.2018.11.023, URL https://doi.org/10.1016/j.jsv.2018.11.023.
- [39] Wilson, A. G., "Eigen Analysis in General Curvilinear Coordinates for Prediction of Noise Propagation in Aeroengine Inlets," 23rd AIAA/CEAS Aeroacoustics Conference, 2017. https://doi.org/10.2514/6.2017-3704, URL https://arc.aiaa.org/doi/abs/10.2514/6.2017-3704.
- [40] Wilson, A. G., "Non-linear acoustic propagation in circumferentially non-uniform mean flow," 25th AIAA/CEAS Aeroacoustics Conference, 2019. https://doi.org/10.2514/6.2019-2448.
- [41] Pickett, G. F., and Sofrin, T. G., "Multiple pure tone noise generated by fans at supersonic tip speeds," *Pennsylvania State Univ. Fluid Mech., Acoustics, and Design of Turbomachinery, Pt.* 2, 1970.
- [42] Hawkings, D., "Multiple tone generation by transonic compressors," *Journal of Sound and Vibration*, Vol. 17, No. 2, 1971, pp. 241–250. https://doi.org/10.1016/0022-460X(71)90458-5.
- [43] Achunche, I., Astley, R. J., Sugimoto, R., and Kempton, A., "Prediction of Forward Fan Noise Propagation and Radiation from Intakes," 15th AIAA/CEAS Aeroacoustics Conference (30th AIAA Aeroacoustics Conference), AIAA, 2009.
- [44] Sanjosé, M., Moreau, S., Pestana, M., and Roger, M., "Effect of weak outlet-guide-vane heterogeneity on rotor-stator tonal noise," *AIAA Journal*, Vol. 55, No. 10, 2017, pp. 3440–3457. https://doi.org/10.2514/1.J055525.

- [45] Peake, N., and Parry, A. B., "Modern challenges facing turbomachinery aeroacoustics," *Annual Review of Fluid Mechanics*, Vol. 44, 2011, pp. 227–248. https://doi.org/10.1146/annurev-fluid-120710-101231.
- [46] James, A. O., "Buzz-Saw Noise Prediction for Axisymmetric and Drooped Turbofan Intakes by," Ph.D. thesis, University of Southampton, 2020.
- [47] Sugimoto, R., James, A. O., McAlpine, A., and Astley, R. J., "CFD/CAA coupling for the prediction of fan tone noise propagation and radiation through a drooped intake," 28th AIAA/CEAS Aeroacoustics Conference, 2022, 2022, pp. 1–15. https://doi.org/10.2514/6.2022-3100.
- [48] Winkler, J., Aaron Reimann, C., Reba, R., and Gilson, J., "Turbofan inlet distortion noise prediction with a hybrid CFD-CAA approach," 20th AIAA/CEAS Aeroacoustics Conference, Vol. 3, No. June, 2014. https://doi.org/10.2514/6.2014-3102.
- [49] Wilson, A. G., "A Method for Deriving Tone Noise Information from CFD Calculations on the Aeroengine Fan Stage," *RTO AVT Symposium on "Ageing Mechanism and Control: Part A Developments in Computational Aero- and Hydro-Acoustics"*, 2001.
- [50] Astley, R. J., Sugimoto, R., Gabard, G., Norde, E., Grift, E. J., and Bocquier, M., "The effect of steady flow distortion on mode propagation in a turbofan intake," 20th AIAA/CEAS Aeroacoustics Conference, 2014, pp. 1–22. https://doi.org/10.2514/6.2014-3113.
- [51] Wu, L., Wilson, A. G., Kim, J. W., Radford, D., and Shahpar, S., "Low-noise blade design optimization for a transonic fan using adjoint-based approach," *AIAA Journal*, Vol. 60, No. 4, 2022, pp. 2367–2382. https://doi.org/10.2514/1.J060959.
- [52] Wu, L., Kim, J.-W., Wilson, A. G., and Shahpar, S., "Automatic Design Optimization of a Transonic Compressor Rotor for Improving Aeroacoustic and Aerodynamic Performance," *Journal of Turbomachinery*, Vol. 144, No. 8, 2022. https://doi.org/10.1115/1.4053916.
- [53] Colin, Y., Aupoix, B., Boussuge, J. F., and Chanez, P., "Numerical Simulation and Analysis of Crosswind Inlet Flows at Low Mach numbers," Proceedings of the 8th International Symposium on Experimental and Computational Aerothermodynamics of Internal Flows, 2007.
- [54] AGARD, "Air Intakes for High Speed Vehicles," Chapter 2, AGARD advisory report 270, 1991.